Multimedia Tools and Applications
https://doi.org/10.1007/s11042-020-10469-5

1166: ADVANCES OF MACHINE LEARNING IN DATA ANALYTICS AND VISUAL INFORMATION PROCESSING

Diffuse lung disease classification based on texture features and weighted extreme learning machine

Shyla Raj[1] · **B. S. Mahanand**[1] · **D. S. Vinod**[1]

Received: 29 April 2020 / Revised: 6 December 2020 / Accepted: 29 December 2020 /
Published online: 22 January 2021

Abstract

Diffuse lung diseases are a group of chronic disorders that affect the lungs. The highly prevalent lung patterns associated with diffuse lung diseases are emphysema, fibrosis, ground-glass opacity, and micro-nodules. For diffuse lung classification problem, TALISMAN (Texture Analysis of Lung ImageS for Medical diagnostic AssistaNce) is one of the widely studied dataset in the literature. It is observed in the dataset that there exists sample imbalance among different tissue patterns. To address the sample imbalance in the data weighted extreme learning machine classifier is employed in this work. To overcome the intra-class and inter-class variation among the diffuse lung patterns features are extracted using the modified intuitionistic local binary pattern along with Gabor filter bank and grey level co-occurrence matrix. These combined texture features are then used to train the weighted extreme learning machine to classify the diffuse lung patterns. The performance of the proposed approach is compared with the existing works in the literature. The comparison results indicate better performance of the proposed approach for diffuse lung classification with sample imbalance.

Keywords Diffuse lung diseases · Texture features · Intuitionistic local binary pattern · Extreme learning machine · Sample imbalance

✉ B. S. Mahanand
bsmahanand@sjce.ac.in

Shyla Raj
shylaraj@jssstuniv.in

D. S. Vinod
dsvinod@daad-alumni.de

[1] Department of Information Science and Engineering, Sri Jayachamarajendra College of Engineering, JSS Science and Technology University, Mysuru, Karnataka, India

1 Introduction

Diffuse Lung Disease (DLD) or interstitial lung disease is an irreversible condition that affects the lung parenchyma [6]. DLD consists of several lung disorders which are heterogeneous in nature but exhibit similar clinical symptoms. DLD is generally caused by dust, pollens, carcinogens, or auto-immune diseases and leads to difficulty in breathing. Since subjects with DLD exhibit similar clinical symptoms, high resolution computed tomography scans are widely used for accurate diagnosis. Diffuse lung diseases are generally manifested as textural alternations in computed tomography scans of lung parenchyma. The highly prevalent lung patterns associated with diffuse lung disorders are emphysema, fibrosis, ground-glass opacity, and micro-nodules. Figure 1 illustrates two samples each for diffuse lung types along with the healthy lung pattern. From Fig. 1 it is observed that even though there are noticeable visual differences between the tissue types, still there exists a higher variation among appearance within the same tissue type. Thereby early detection of diffuse disease requires identification of subtle changes in texture properties of the lungs.

There is a growing interest in employing texture features for diffuse lung classification using computed tomography images [3, 24]. The texture features widely used in DLD classification include gray-level histogram (GLH), gray-level co-occurrence matrices (GLCM), grey level run length matrix (GLRLM), local binary pattern (LBP), histogram of oriented gradient, Gabor filter bank, and wavelets. One of the early work on diffuse lung classification was based on adaptive multiple feature method proposed by Uppaluri et al. [28]. In [28] texture features from grey-level distribution, run-length, GLCM, and fractal measures were used to train Bayesian classifier and an accuracy of 93.5% was obtained. Vasconcelos et al. [30] classified diffuse lung tissues using features from GLH, GLRLM, spatial grey level dependence, and differential lacunarity and reported an accuracy of 94.5% using support vector machine (SVM). Several studies have employed multi-scale filter bank approach to describe local image structures in lung images [25, 29, 31]. Song et al. [25] employed rotation-invariant Gabor-local binary pattern and multi-coordinate histogram of oriented gradients (HOG) for diffuse lung classification using TALISMAN dataset. An overall F-score of 81% was reported in [25] for DLD classification using patch adaptive sparse approximation technique. Some works have also employed histogram of oriented gradients and local binary pattern (LBP) for extracting local neighborhood features in the lung images

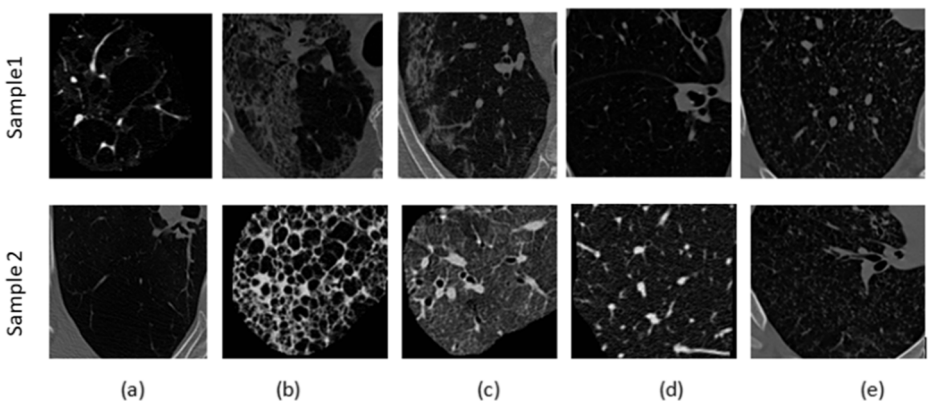

Fig. 1 Two samples of each DLD tissue type **a** emphysema **b** fibrosis **c** ground glass **d** healthy **e** micro-nodules

[25, 26]. Sorensen et al. [26] combined LBP and GLH for classifying the different textures in lung image using k-NN classifier and reported an accuracy of 95.2%. Frequency domain techniques such as isotropic wavelet and Riesz wavelet are also been used for diffuse lung classification [9, 15, 16]. Joyseeree [16] performed multi-class DLD classification on TALISMAN dataset by fusing features from Riesz filter and deep CNN and reported area under curve of 0.95 using softmax classifier. Literature survey clearly indicates that combining multiple texture features handles the heterogeneity in the diffuse lung patterns.

Recently convolutional neural network (CNN) models has been employed for diffuse lung classification [14, 27]. One of the early work using CNN was reported by Anthimopoulos et al. [2] for classifying diffuse lung patterns. In [2] sample imbalance in TALISMAN dataset is addressed by data augmentation techniques namely rotation and flip and an accuracy of 85.6% was obtained. Wang et al. [31] employed multi-scale rotation invariant CNN for DLD classification with Gabor-LBP images and reported an accuracy of 90.1%. Guo et al. [11] proposed kernel DenseNet for DLD classification with an average F-score of 98.4%. Bermejo et al. [4] employed an ensemble deep CNNs by using multi-dimensional architectures and obtained an average sensitivity and specificity of 91.41% and 98.18% respectively. Recently transfer learning based approach and deep CNN models are also being reported for diffuse lung classification [14, 27].

In the literature one of the widely studied and publicly available dataset for diffuse lung classification is TALISMAN (Texture Analysis of Lung ImageS for Medical diagnostic AssistaNce) [8]. It is found in the TALISMAN dataset that there exists imbalance in sample (region of interest patches) distribution among different disease types. Sample imbalance in data is an important problem to be addressed because while training classifiers tend to be biased towards the class with more samples and may affect the accuracy of the class with fewer samples. The sample imbalance can be addressed either by sampling approach or by the algorithmic approach. The sampling approach modifies the data distribution by employing oversampling or undersampling. In contrast, the algorithmic approach does not modify the sample distribution but introduces a cost metric which assigns misclassification cost to each class based on the size of the class. Data augmentation techniques such as rotation and flip were used to increase the sample size and to handle the imbalance in TALISMAN dataset [2, 14]. However, the data augmentation approach may not be appropriate for a medical imbalance problem because it creates synthetic samples.

The main objective of the work is to handle sample imbalance in the TALISMAN dataset using weighted extreme learning machine (WELM) classifier. WELM handles the imbalance in the class distribution by automatically generating the misclassification cost matrix [34]. To overcome the intra-class and inter-class variations among the diffuse lung patterns features are extracted using modified intuitionistic local binary pattern (MILBP) along with the Gabor filter bank and grey level co-occurrence matrix. The proposed MILBP is based on intuitionistic fuzzy approach and it deals with the uncertainty in the traditional fuzzy approach by including hesitation degree along with membership and non-membership values. The extracted texture features are then used as an input to the WELM classifier to distinguish between healthy and disease types. To the best of our knowledge, none of the DLD classifications in the literature have addressed the sample imbalance in the TALISMAN dataset using machine learning approach.

The paper is organized as follows: Section 2 describes the dataset used in the work, MILBP and WELM classifier. Section 3 presents the results of the proposed approach and performance comparison with the existing works. The main conclusions of the work are summarized in Section 4.

2 Material and methods

In this work diffuse lung disease classification using texture features and WELM classifier is proposed. The overall framework of the proposed approach is shown in Fig. 2. DLD image patches of different tissue types namely emphysema, ground-glass opacity, micro-nodules, fibrosis, and healthy are used from the TALISMAN benchmark dataset. Texture features are extracted from DLD patches using the modified intuitionistic local binary pattern (MILBP) along with the Gabor filter bank and grey level co-occurrence matrix (GLCM). The combined texture features are then used as the input to the weighted extreme learning machine (WELM) to classify the healthy and disease types.

2.1 Dataset

The publicly available TALISMAN benchmark dataset is used for DLD classification [8]. The dataset consists of 103 image series of DLD types that include emphysema, ground-glass opacity, micro-nodules, fibrosis, and healthy. A total of 1363 two-dimensional annotated Region of Interest (ROI) have been annotated by experienced radiologists. From these annotated ROIs, 14,356 overlapping patches of size 32×32 are extracted to represent the DLD pattern. The TALISMAN dataset also consists of various clinical parameters such as age, gender, smoking history, disease duration, and many others. The distribution of the number of images, annotated ROIs, and patches used in the study are detailed in Table 1.

2.2 Texture feature extraction

Diffuse lung disease classification is a challenging task because of high intra-class and low inter-class differences among the patterns. The success of DLD classification mainly depends on the extracted texture features. Since DLD patterns are divergent in nature, a single texture feature may not effectively classify all diffuse types as reported in the literature [15, 25]. In this work, texture features are extracted using the MILBP along with the Gabor filter bank and GLCM.

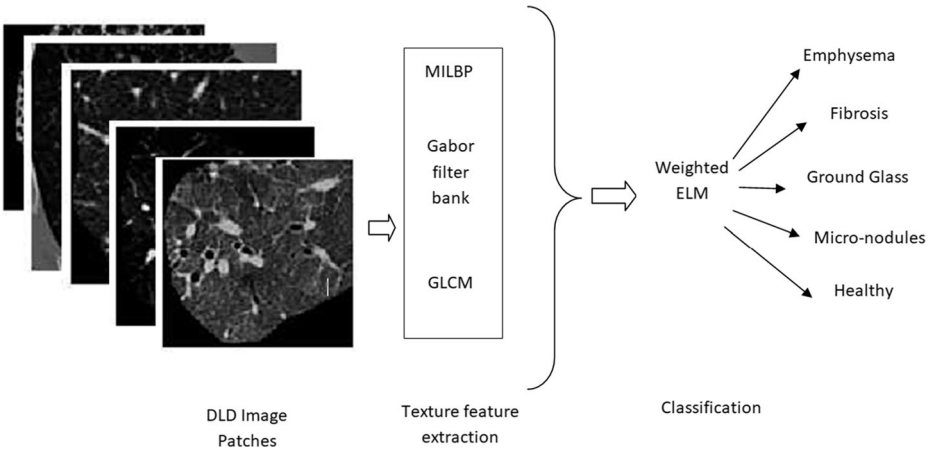

Fig. 2 Framework of the proposed approach

Table 1 The per-class distribution of DLD tissue types

Diffuse lung disease type	No. images	No. annotated ROI	No. Samples(patches)
Emphysema (E)	5	66	1177
Ground Glass (G)	37	427	2226
Micro-nodules (MN)	16	297	2384
Fibrosis (F)	38	473	3039
Healthy (H)	7	100	5530
Total	103	1363	14,356

2.2.1 Modified intuitionistic fuzzy local binary pattern (MILBP)

In this work modified intuitionistic fuzzy local binary pattern (MILBP) is proposed for extracting texture features from diffuse lung images. The traditional local binary pattern (LBP) is a non-parametric greyscale rotation-invariant texture descriptor [19]. LBP is based on a hard threshold where the pixel-wise comparison is performed between the center pixel P_c and neighboring pixels P_i in an NXN neighborhood. However, in presence of high noise and low contrast LBP may fail to extract prominent features because of hard thresholding. Naresh and Nagendraswamy proposed a modified approach for LBP based on fuzzy membership function [18]. However, in the case of hesitancy originating from imperfect or imprecise information in defining fuzzy membership function, the modified fuzzy approach may not be appropriate to apply. Recently Ansari and Ghrera reported intuitionistic fuzzy local binary approach [1]. In their work finding an optimal pair of threshold and hesitation value requires several iterations and is computationally expensive. To overcome these shortcomings, in this work MILBP is proposed by incorporating intuitionistic fuzzy properties. The MILBP deals with uncertainty in the traditional fuzzy technique by including the hesitation along with membership and non-membership values.

In the MILBP approach, the membership value $\mu_{Tr}(z_{ij})$ of pixels in 3 × 3 window is calculated using the fuzzy triangular membership function. The fuzzy triangular membership function is defined by three values x, y, z where x, z are extreme points of the triangle, and y is the midpoint of the triangle [22]. P_i represents the intensities of the pixels in the neighborhood 3 × 3, P_c represents the intensity of the center pixel, and 'N' is the number of neighbors in the window.

The mean and standard deviation of pixels contained in 3 × 3 neighbourhood is computed as follows:

$$\mu = \frac{\sum_{i=1}^{N} P_c + P_i}{(N+1)} \tag{1}$$

$$\sigma = \sqrt{\frac{(P_c - \mu)^2 + \sum_{i=1}^{N} (P_i - \mu)^2}{(N+1)}} \tag{2}$$

The values of x, y, and z of the fuzzy triangle are defined as

$$x = \mu - \sigma \tag{3}$$

$$y = \mu \tag{4}$$

$$z = \mu + \sigma \tag{5}$$

After defining the fuzzy triangle, the fuzzy triangular membership value of 3 × 3 neighborhood is defined as:

$$\mu_{Tr}(z_{ij}) = \begin{cases} \frac{P_i - x}{y - x} & \text{if } x \leq P_i \leq y \\ \frac{z - P_i}{z - y} & \text{if } y \leq P_i \leq z \\ 0 & \text{otherwise} \end{cases} \tag{6}$$

After computing the membership value $\mu_{Tr}(z_{ij})$, the next step involves calculating the non-membership value $v_{Tr}(z_{ij})$ of the 3 × 3 neighbourhood. By experimentation, it is found that Sugeno's and Yager's generators are not successful in satisfying the elementary condition of intuitionism in our case. So the non-membership value $v_{Tr}(z_{ij})$ of the 3 × 3 neighbourhood is defined using Bustince fuzzy complement [5]. The non-membership value $v_{Tr}(z_{ij})$ is calculated as :

$$v_{Tr}(z_{ij}) = 1 - ((1 - \mu_{Tr}(z_{ij})^{\lambda})^{\frac{1}{\lambda}}, \lambda > 0 \tag{7}$$

The hesitation degree $\pi_{Tr}(z_{ij})$ is calculate as :

$$\pi_{Tr}(z_{ij}) = 1 - \mu_{Tr}(z_{ij}) - v_{Tr}(z_{ij}) \tag{8}$$

The membership function $\mu_{If}(z_{ij})$ of MILBP is given as the combination of fuzzy triangular membership function $\mu_{Tr}(z_{ij})$ and the hesitation degree $\pi_{Tr}(z_{ij})$

$$\mu_{If}(z_{ij}) = \mu_{Tr}(z_{ij}) + \pi_{Tr}(z_{ij}) \tag{9}$$

The pixels in the 3 × 3 neighborhood are modified according to μ_{If}. Then the pixel wise comparison is performed between center pixel P_c and neighbouring pixel P_i and is represented by a binary value (B) as shown below :

$$B = \begin{cases} 1 & \text{if } P_i \geq P_c \\ 0 & \text{otherwise} \end{cases} \tag{10}$$

The binary value B is multiplied with the corresponding binary weight of the 3 × 3 window to obtain the value of the center pixel P_c.

$$MILBP = \sum_{i=0}^{N} B * 2^{i-1} \tag{11}$$

The histogram of MILBP values obtained from (11) is considered as the texture features of diffuse lung image.

2.2.2 Gabor filter bank

The Gabor filter bank is multi-scale, multi-directional and rotation-invariant texture analysis method [7, 12]. The scales 'S' and orientation 'R' is represented as $S = 0, 1, \ldots S - 1$ and $R = 0, 1, \ldots R - 1$ respectively. To obtain rotation invariant response the oriented filter responses at each scale is averaged. The final feature vector is built by including energies (E) and standard deviations (σ) of all rotation invariant responses obtained at each scale. A set of Gabor-filtered images $\{I^{s,r}\}$ is estimated by convolving an image I(x,y) with each Gabor function. The rotation-invariant Gabor-filtered images $I^s(x, y)$ are acquired by summing all 'R' Gabor functions of certain scale 'S':

$$I^s(x, y) = \sum_{r=0}^{R-1} I^{\{s,r\}}(x, y) \tag{12}$$

2.2.3 Grey level co-occurrence matrix (GLCM)

GLCM is used in this work to analyze the spatial distribution of pixel intensities in the image. GLCM is a two-dimensional matrix which provides information regarding how frequently pixel with intensity 'x' appear in specific spatial relationship with pixel with intensity 'y' [13]. Nine features namely energy, entropy, correlation, autocorrelation, contrast, variance, homogeneity, dissimilarity, and sum average are extracted from the two-dimensional matrix.

The texture features extracted from the modified intuitionistic fuzzy local binary pattern, Gabor filter bank, and grey level co-occurrence matrix are combined and then used as an input to weighted extreme learning machine classifier to classify between healthy and DLD types.

2.3 Weighted Extreme Learning Machine for sample imbalance learning

Weighted Extreme Learning Machine (WELM) is a cost-sensitive classifier capable of handling class imbalance problem [34] and has been employed in many practical classification problems [17, 32, 33]. WELM is a single layer feed-forward neural network which as a random generation of hidden nodes independent of training samples and hidden layer output. WELM handles imbalance in the class distribution by automatically generating the misclassification cost matrix. The misclassification cost for a class is inversely proportional to the number of samples in the respective class. By associating higher misclassification cost the strength of the minority class is enhanced while lower misclassification cost weakens the relative impact of the majority class. The WELM belongs to the class of cost-sensitive learning because weights are associated with each sample in the dataset.

WELM tries to minimize the training error ξ_j and maximize the marginal distance between the classes $\| \beta \|/2$. Mathematically this optimization is written as:

$$Minimize : L_{WELM} = \frac{\|\beta\|^2}{2} + \frac{1}{2} CW \sum_{j=1}^{M} \|\xi_j\|^2 \tag{13}$$

$$Subjectto : h(y_j)\beta = {t_j}^T - {\xi_j}^T, i = i, \ldots, M \tag{14}$$

where C is the regularization parameter representing the trade-off between the minimization of training errors and the maximization of the marginal distance. W is the weight matrix of size MxM where M is the number of samples. W is a matrix of zeros, with a diagonal representing the misclassification cost. The weight matrix W determines the degree of re-balance the users are seeking and how much further the boundary is pushed towards the class with majority samples. There are two weighting schemes $W1$ and $W2$ based on the degree of re-balancing.

$$Weighting\ Scheme \quad W1 \ : W_i = \frac{1}{No.(t_i)} \tag{15}$$

where $No.(t_i)$ is the number of samples in the class t_i, i = 1...M. Weighting scheme W1 re-balances the minority class and majority class in the ratio $\underbrace{1 : 1 : \cdots 1}_{M}$.

The weighting scheme W2 re-balances the minority class and majority class in the ratio 0.618:1 and is represented as:

$$Weighting\ Scheme \quad W2 = \begin{cases} W_i = 0.618/No.(t_i) & if \ \ t_i > AVG(t_i) \\ W_i = 1/No.(t_i) & if \ \ t_i \leq AVG(t_i) \end{cases} \tag{16}$$

For a multi-class problem, the class with samples below the average samples is referred to as minority class, and the class with samples above the average samples is the majority class. The performance of the WELM is mainly dependent on Gaussian activation function parameters viz 'σ' the kernel value and 'C' the trade-off constant. In this work, a grid search approach is used to obtain optimal values for 'σ' and 'C' to train the WELM classifier. The 'σ'(2^{14}), 'C' value (2^{28}) and weighing scheme W1 is used for classification. The WELM training model is explained in Algorithm 1. The training phase involves determining the output weight β in the testing phase using the β the class labels of the unknown samples are determined.

Algorithm 1 WELM algorithm.

Data: Given a set of training data D = $\{(x_i, t_i) | \ x_i \epsilon R^n, t_i \epsilon R^m, \forall$ i = 1...M $\}$
Activation function g(x) and number of hidden nodes 'L'

Result: Trained WELM model

Step 1: Define the weight matrix 'W' associated with each training sample x_i according to (15) or (16)

Step 2: Randomly generate input weight vector w_i and hidden node bias b_i, i=1...M.

Step 3: Compute hidden layer output matrix 'H' as

$$\mathrm{H} = (w_1 \ldots w_L, b_1 \ldots b_L, x_1 \ldots x_L)$$

$$\begin{bmatrix} g(w_1, b_1, x_1) \ldots g(w_L, b_L, x_1) \\ \vdots \qquad\qquad \vdots \\ g(w_1, b_1, x_M) \ldots g(w_L, b_L, x_M) \end{bmatrix}_{MXL} \tag{17}$$

Step 4: Calculate Output weight $\beta : \beta = H^{\dagger} T$ as

$$\beta = H^T \left(\frac{1}{c} + WHH^T \right)^{-1} WT \tag{18}$$

where T = $[t_1 \ldots t_M]$

$H^{\dagger}$ is Moore-Penrose generalized inverse of hidden layer output matrix 'H'

3 Experimental results

3.1 Sample imbalance in TALISMAN dataset

TALISMAN dataset used in this work consists of lung patterns from emphysema, ground-glass opacity, micro-nodules, fibrosis, and healthy [8]. The per-class sample (ROI patch) distribution is detailed in Table 1. The sample distribution of the dataset is graphically presented in Fig. 3. From Fig. 3 it is observed that the emphysema class consists of 1177

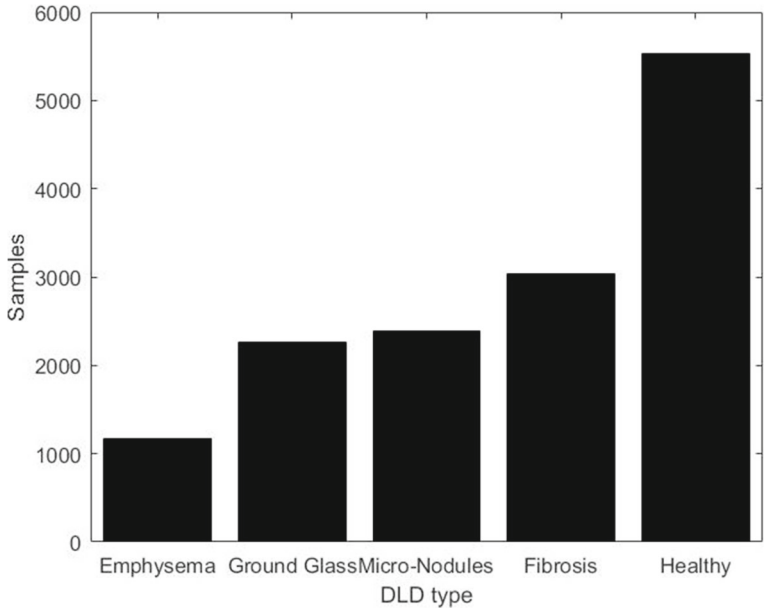

Fig. 3 Graphical representation of TALISMAN dataset

patches whereas, the healthy class has 5530 patches. It is also observed that there is variation in sample distribution among the other three classes compared to healthy. The imbalance degree of the TALISMAN dataset is quantitatively measured using an imbalance ratio (IR). IR is the ratio of the number of samples in the minority class to the number of samples in the majority class. IR for the multi-class problem is given as:

$$IR = \frac{No.Minclass(tr_i)}{No.Maxclass(tr_i)} i = 1...n \tag{19}$$

where tr_i is the training samples.

Applying (19) it is found that the TALISMAN dataset has an IR ratio of 0.21 which indicates the high difference in sample distribution between majority class (healthy) and minority class (emphysema).

3.2 Evaluation metric

In most of the classification problems performance is evaluated using accuracy measure. However, in the case of sample imbalance in data distribution, accuracy may not be an appropriate metric to measure the performance of the classifier. Since the TALISMAN dataset has an imbalanced sample distribution, the performance of the WELM classifier is evaluated using precision, recall, F-score, and G-mean measures. Precision, recall, F-score, and G-mean is measured as follows:

$$Precision = \frac{TP}{TP + FP} \tag{20}$$

$$Recall = \frac{TP}{TP + FN} \tag{21}$$

$$F - score = \frac{2TP}{2TP + FP + FN} \tag{22}$$

$$G - mean = \sqrt{\frac{TP}{TP + FN} X \frac{TN}{TN + FP}} \tag{23}$$

where TP is True Positive, TN is True Negative, FP is False Positive, and FN is False Negative.

Precision measures the percentage of the relevant results, and recall measures the percentage of total relevant results that are classified correctly. F-score is the harmonic average of the precision and recall and is the measure of the test's accuracy. It can be observed from eq (22) that F-score does not take into consideration True Negative (TN) scores. To take into account the TN scores and to evaluate the classification performance in the sample imbalance scenario, G-mean is used in the work.

3.3 Performance evaluation

The classification performance of the WELM classifier is evaluated in terms of precision, recall, F-score, G-mean, and receiver operating characteristic (ROC) curve. TALISMAN benchmark dataset has 14,356 ROI patches. The experiments are conducted by splitting the dataset into 70% training and 30% testing. For better generalization experiments are repeated ten times with different random combinations with stratification. The texture features viz. modified intuitionistic fuzzy local binary pattern, Gabor filter bank, and grey level co-occurrence matrix are combined and fed as an input to the WELM classifier. Table 2 presents the classifier performance for each lung tissue type. From Table 2 it is observed G-mean of ground glass is 0.93, micro-nodules is 0.91, fibrosis is 0.91, healthy is 0.93 and for highly imbalanced emphysema class G-mean is 0.86. For all DLD classes the mean precision of 0.87, recall of 0.85, F-score of 0.86, and G-mean of 0.91 is obtained using the WELM classifier. Additionally ROC curve is generated for better interpretation of the results. ROC curve for WELM classifier is shown in Fig. 4. From Fig. 4 it is observed that area under the curve obtained for emphysema is 0.87, fibrosis is 0.92, ground glass is 0.92, micro-nodules is 0.93, and 0.93 for healthy.

Recently some studies have reported handling class imbalance using twin SVM approach for general classification problem [20, 21]. The performance of the WELM classifier is compared with robust energy-based least squares twin support vector machine (RELS-TSVM) and least squared support vector machine (LS-SVM) classifiers and is shown in Table 3. From Table 3 it is observed that WELM resulted in a G-mean of 0.86 for highly imbalanced emphysema class compared to G-mean of 0.84 from RELS-TSVM and 0.76 from LS-SVM. For all DLD classes an overall G-mean of 0.91 is obtained by WELM,

Table 2 Classification performance of WELM classifier

DLD Type	Precision	Recall	F-score	G-mean
Emphysema	0.81	0.75	0.78	0.86
Ground Glass	0.84	0.89	0.86	0.93
Micro Nodules	0.88	0.85	0.87	0.91
Fibrosis	0.95	0.84	0.89	0.91
Healthy	0.88	0.94	0.91	0.93
Mean	0.87	0.85	0.86	0.91

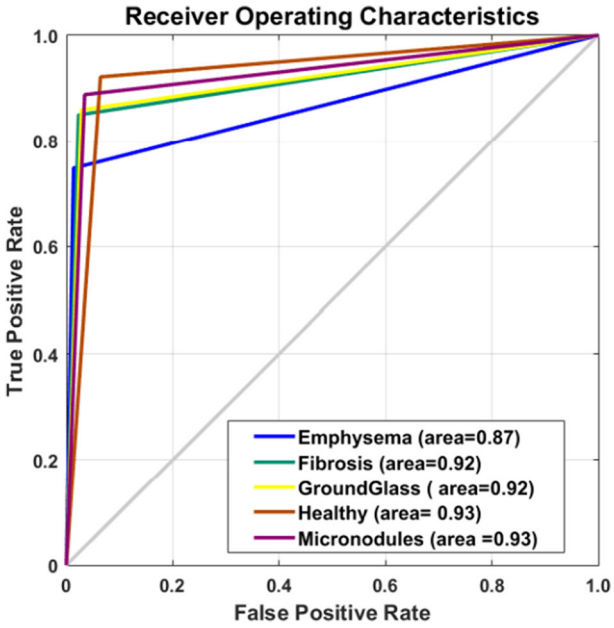

Fig. 4 ROC curves and respective AUC of WELM classifier

0.89 by RELS-TSVM, and 0.88 by LS-SVM. The result comparison indicates that WELM achieves a performance improvement of around 3%.

3.4 Performance comparison with existing works

The results of WELM classifier is compared with Riesz wavelet-based texture analysis and SVM [15], rotation-invariant Gabor-LBP and multi-coordinate HOG gradients descriptor using patch adaptive sparse approximation [25], isotropic wavelet-based SVM [9] and recent deep CNN models [10, 16, 23]. It has been found that in most of the existing works sample imbalance present in TALISMAN is handled by data augmentation techniques such as rotation, flip, and translation. However, the synthetic samples generated by data augmentation techniques may not be appropriate for medical data. In this work, sample imbalance is handled using the cost-sensitive WELM classifier without generating synthetic samples. The class-wise recall comparison of WELM classifier with existing works in the literature is shown in Table 4. The results from Table 4 shows that the proposed approach produces

Table 3 Performance comparison of WELM with RELS-TSVM and LS-SVM classifier

DLD Type	WELM	RELS-TSVM	LS-SVM
Emphysema	0.86	0.84	0.76
Ground Glass	0.93	0.92	0.89
Micro Nodules	0.91	0.91	0.89
Fibrosis	0.91	0.92	0.93
Healthy	0.93	0.90	0.92
G-Mean	0.91	0.89	0.88

Table 4 The class-wise recall comparison of proposed approach with existing works in the literature

Method	E	GG	MN	F	H
Proposed	**0.75**	**0.89**	**0.85**	**0.84**	**0.94**
Joyseeree et al. [16]	0.54	0.77	0.81	0.88	0.63
Joyseeree et al. [15]	0.57	0.73	0.88	0.82	0.73
Gao et al. [10]	0.83	0.82	0.88	0.89	0.91
Shin et al. [23]	0.91	0.70	0.79	0.83	0.68
Song et al. [25]	0.81	0.83	0.81	0.81	0.88
Depeursinge et al. [9]	0.78	0.81	0.81	0.81	0.59

better class-wise recall for ground glass (GG) and healthy (H) patterns compared to other existing works. For other DLD classes the performance of the proposed approach is similar to other works.

4 Conclusion

In this work the sample imbalance in diffuse lung classification is handled by employing the weighted extreme learning machine classifier. The inter and intra class variations among the lung patterns is addressed by extracting texture features using the modified intuitionistic local binary pattern along with Gabor filter bank, and grey level co-occurrence matrix. The weighted extreme learning machine classifier is trained using the extracted texture features to distinguish between healthy and disease types. The performance results indicate that WELM produced a mean recall of 0.85, precision 0.87, F-score of 0.86, and G-mean of 0.91. The results of WELM are compared with recent robust energy-based least squares twin support vector machine and least squared support vector machine classifiers and an overall performance improvement of around 3% is obtained. The study clearly indicates that by using texture features and handling sample imbalance by employing the WELM classifier better classification performance can be achieved for diffuse lung diseases.

References

1. Ansari MD, Ghrera SP (2018) Intuitionistic fuzzy local binary pattern for features extraction. Int J Inf Commun Technol 13(1):83–98
2. Anthimopoulos M, Christodoulidis S, Ebner L, Christe A, Mougiakakou S (2016) Lung pattern classification for interstitial lung diseases using a deep convolutional neural network. IEEE Trans Med Imaging 35(5):1207–1216
3. Bağcı U, Bray M, Caban J, Yao J, Mollura DJ (2012) Computer-assisted detection of infectious lung diseases: a review. Comput Med Imaging Graph 36(1):72–84
4. Bermejo-Peláez D, Ash SY, Washko GR, Estépar RSJ, Ledesma-Carbayo MJ (2020) Classification of interstitial lung abnormality patterns with an ensemble of deep convolutional neural networks. Sci Rep 10(1):1–15
5. Bustince H, Kacprzyk J, Mohedano V (2000) Intuitionistic fuzzy generators application to intuitionistic fuzzy complementation. Fuzzy Sets Syst 114(3):485–504
6. Dalpiaz G, Maffessanti M (2013) Diffuse lung diseases. In: Geriatric imaging. Springer, pp 365–388
7. Dash JK, Mukhopadhyay S, Gupta RD (2017) Multiple classifier system using classification confidence for texture classification. Multimed Tools Appl 76(2):2535–2556

8. Depeursinge A, Vargas A, Platon A, Geissbuhler A, Poletti PA, Müller H (2012) Building a reference multimedia database for interstitial lung diseases. Comput Med Imaging Graph 36(3):227–238
9. Depeursinge A, Van de Ville D, Platon A, Geissbuhler A, Poletti PA, Muller H (2012) Near-affine-invariant texture learning for lung tissue analysis using isotropic wavelet frames. IEEE Trans Inf Technol Biomed 16(4):665–675
10. Gao M, Bagci U, Lu L, Wu A, Buty M, Shin HC, Roth H, Papadakis GZ, Depeursinge A, Summers RM et al (2018) Holistic classification of ct attenuation patterns for interstitial lung diseases via deep convolutional neural networks. Comput Methods Biomech Biomed Eng: Imaging Visual 6(1):1–6
11. Guo W, Xu Z, Zhang H (2019) Interstitial lung disease classification using improved densenet. Multimed Tools Appl 78(21):30615–30626
12. Han J, Ma KK (2007) Rotation-invariant and scale-invariant gabor features for texture image retrieval. Image Vis Comput 25(9):1474–1481
13. Haralick RM, Shanmugam K et al (1973) Textural features for image classification. IEEE Trans Syst Man Cybern (6):610–621
14. Huang S, Lee F, Miao R, Si Q, Lu C, Chen Q (2020) A deep convolutional neural network architecture for interstitial lung disease pattern classification. Med Biol Eng Comput 58(4):725–737
15. Joyseeree R, Müller H, Depeursinge A (2018) Rotation-covariant tissue analysis for interstitial lung diseases using learned steerable filters: performance evaluation and relevance for diagnostic aid. Comput Med Imaging Graph 64:1–11
16. Joyseeree R, Otálora S, Müller H, Depeursinge A (2019) Fusing learned representations from riesz filters and deep cnn for lung tissue classification. Med Image Anal 56:172–183
17. Li L, Sun R, Cai S, Zhao K, Zhang Q (2019) A review of improved extreme learning machine methods for data stream classification. Multimed Tools Appl 78(23):33375–33400
18. Naresh Y, Nagendraswamy H (2016) Classification of medicinal plants: an approach using modified lbp with symbolic representation. Neurocomputing 173:1789–1797
19. Ojala T, Pietikainen M, Maenpaa T (2002) Multiresolution gray-scale and rotation invariant texture classification with local binary patterns. IEEE Trans Pattern Anal Mach Intell 24(7):971–987
20. Richhariya B, Tanveer M (2018) A robust fuzzy least squares twin support vector machine for class imbalance learning. Appl Soft Comput 71:418–432
21. Richhariya B, Tanveer M (2020) A reduced universum twin support vector machine for class imbalance learning. Pattern Recognit 102:107–150
22. Ross TJ (2005) Fuzzy logic with engineering applications. Wiley, New York
23. Shin HC, Roth HR, Gao M, Lu L, Xu Z, Nogues I, Yao J, Mollura D, Summers RM (2016) Deep convolutional neural networks for computer-aided detection: Cnn architectures, dataset characteristics and transfer learning. IEEE Trans Med Imaging 35(5):1285–1298
24. Sluimer I, Schilham A, Prokop M, Van Ginneken B (2006) Computer analysis of computed tomography scans of the lung: a survey. IEEE Trans Med Imaging 25(4):385–405
25. Song Y, Cai W, Zhou Y, Feng DD (2013) Feature-based image patch approximation for lung tissue classification. IEEE Trans Med Imaging 32(4):797–808
26. Sorensen L, Shaker SB, De Bruijne M (2010) Quantitative analysis of pulmonary emphysema using local binary patterns. IEEE Trans Med Imaging 29(2):559–569
27. Sukanya Doddavarapu V, Kande GB, Prabhakara Rao B (2020) Differential diagnosis of interstitial lung diseases using deep learning networks. Imaging Sci J 1–9
28. Uppaluri R, Hoffman EA, Sonka M, Hartley PG, Hunninghake GW, McLennan G (1999) Computer recognition of regional lung disease patterns. Am J Respir Crit Care Med 160(2):648–654
29. van Ginneken B, ter Haar Romeny BM (2003) Multi-scale texture classification from generalized locally orderless images. Pattern Recognit 36(4):899–911
30. Vasconcelos V, Barroso J, Marques L, Silvestre Silva J (2015) Enhanced classification of interstitial lung disease patterns in hrct images using differential lacunarity. BioMed Res Int 2015:1–9
31. Wang Q, Zheng Y, Yang G, Jin W, Chen X, Yin Y (2018) Multiscale rotation-invariant convolutional neural networks for lung texture classification. IEEE J Biomed Health Inform 22(1):184–195
32. Xu Z, Liu J, Luo X, Yang Z, Zhang Y, Yuan P, Tang Y, Zhang T (2019) Software defect prediction based on kernel pca and weighted extreme learning machine. Inf Softw Technol 106:182–200
33. Zhang J, Wang H, Ren Y (2019) Robust tracking via weighted online extreme learning machine. Multimed Tools Appl 78(21):30723–30747
34. Zong W, Huang GB, Chen Y (2013) Weighted extreme learning machine for imbalance learning. Neurocomputing 101:229–242